Thin Solid Films 761 (2022) 139536

Contents lists available at ScienceDirect

Thin Solid Films

journal homepage: www.elsevier.com/locate/tsf

Vertically-aligned *p-n* junction Si solar cells with CdTe/CdS luminescent solar convertors

M. Semenenko [a], M. Dusheiko [b], G. Okrepka [c,d], R. Redko [a,e,*], S. Antonin [a], V. Hladkovskyi [f], V. Shvalagin [g], F. Gao [h], S. Shahan [b], A. Sarikov [a]

[a] *V. Lashkaryov Institute of Semiconductor Physics of the National Academy of Sciences of Ukraine, 41 Nauky Avenue, Kyiv 03028, Ukraine*
[b] *National Technical University of Ukraine "Igor Sikorsky Kyiv Polytechnic Institute", 37 Peremohy Avenue, Kyiv 03056, Ukraine*
[c] *Institute of Biology, Chemistry and Bioresources, Yuriy Fedkovych Chernivtsi National University, 2 Kotsjubynskyi Street, Chernivtsi 58012, Ukraine*
[d] *Bukovinian State Medical University, 2 Teatralna Square, Chernivtsi 58000, Ukraine*
[e] *State University of Telecommunications, 7 Solomenska Street, Kyiv 03110, Ukraine*
[f] *Plasma Physics and Plasma Technology Department, Institute for Nuclear Research of the National Academy of Sciences of Ukraine, 47 Nauky Avenue, Kyiv 03028, Ukraine*
[g] *L. Pysarzhevskiy Institute of Physical Chemistry of the National Academy of Sciences of Ukraine, 31 Nauky Avenue, Kyiv 03028, Ukraine*
[h] *South China Normal University, 55 West of Zhongshan Avenue, Tianhe District, Guangzhou 510631, China*

ARTICLE INFO

Keywords:
Luminescence down-shifting
Solar cell
Cadmium telluride
Cadmium sulfide
Nanocrystals
Nanoparticles

ABSTRACT

In this work, flat solar cells with vertically aligned *p-n* junctions are designed. Luminescent down-shifting layers are used for enhancement of the solar cells' efficiency. The solar cells are fabricated with the architecture of double aligned *p-n* junctions and contain additional coatings with CdTe/CdS luminescent nanocrystals. Current-voltage characteristics of the solar cells are measured using a solar simulator with a pulsed halogen light source. The influence of the average diameter of the CdTe/CdS nanocrystals in the series of 2.8, 3.6 and 4 nm and related to its emission at the wavelengths of 548, 609, and 642 nm, respectively, on the solar cells' efficiency is studied and discussed. A flat solar cell with vertically aligned *p-n* junctions containing luminescent down-shifting layers of the nanocrystals that are 4.0 nm in diameter demonstrates a power conversion efficiency of 9% on an area of 1cm^2.

1. Introduction

Photovoltaic electricity (PE) is one of the most promising solutions to build an oil-independent society. A design concept of solar cells (SCs) with luminescent solar concentrators (LSCs) proposed several decades ago [1–6] offers a modern way to produce cost-effective SCs. LSCs were introduced in 1976 by Weber and Lambe [7]. An LSC is a transparent slab containing particles or nanocrystals (NCs) that re-emit absorbed incident light. Generally, such slab is designed as a windowpane mounted together with the SC elements that can be installed at the slab edges. In such alignment, a portion of incident photon flux focuses on the SC, while the rest of the flux passes through the window penetrating inside the building. Such concept of "adaptive windows" [8] can be easily integrated in a building's construction. LSC operation is based on the internal reflection of light re-emitted by the NCs in the transparent film. An LSC absorbs photons with the energies corresponding to a major part of the spectrum of incident sunlight and re-emits photons with lower energies, as compared to the incident ones. The re-emitted light is reflected multiple times by the NCs and is partially redistributed to the edges of the LSC where it is concentrated. In such case, the collecting edge area is smaller than the receiving one, which enables sunlight concentration without solar tracking. Theoretically, about 75–80% of NC luminescence would be trapped due to the total internal reflection in the LSC as reported in [9]. In such design of SC modules, each SC element may be coupled to one or more edges of the LSC slab to receive the concentrated light [10,11]. Such an arrangement should lead to a substantial decrease of the number of SCs needed to produce a given amount of PE and result in cost-effective SC modules. The collecting power conversion efficiency (PCE) can reach 20%, whereas "adaptive windows" for buildings would remain semitransparent [9]. For instance,

* Corresponding author at: V. Lashkaryov Institute of Semiconductor Physics of the National Academy of Sciences of Ukraine, 41 Nauky Avenue, Kyiv 03028, Ukraine.
E-mail address: redko.rom@gmail.com (R. Redko).

https://doi.org/10.1016/j.tsf.2022.139536
Received 12 April 2022; Received in revised form 3 October 2022; Accepted 5 October 2022
Available online 7 October 2022

PCE of SCs equal to 2.63% was reported in [12]. In this work, "adaptive windows" were designed based on silicon SCs and LSC slabs containing N-doped carbon dots/polymethylmethacrylate (PMMA). An alternative approach to improve the PCE of SCs consists in using tandem LSCs. To realize such LSCs, two materials with quantum dots (QDs) having different optical characteristics are required. In [13], a slab containing Mn^{2+} doped $Cd_xZn_{1-x}S/ZnS$ QDs was used as the top layer and $CuInSe_2/ZnS$ QDs as the bottom layer. The top layer absorbed ultraviolet light, while the bottom layer absorbed the near-infrared part of incident light. Properties of LSC slabs with NCs or luminophores, as well as an increase of the record PCE of SCs were reviewed in detail [1,2]. The highest PCE of an SC ever reported amounts to 7.1% [2,13,14]. A module with four parallel connected SCs based on GaAs with the dimensions of 0.050 m × 0.050 m × 0.005 m was designed. SCs were coupled to the edges of a PMMA LSC slab containing a mixture of two organic dye luminophores.

Alternatively, concentration of light in target areas can be achieved by using up and down wavelength convertors, as was reported in [15–18]. In contrast to "adaptive windows", the proposed design concept [18] uses luminescent down-shifting layers (LDSLs). LDSLs were combined with crystalline Si or thin films containing CdTe/CdS core-shell NCs in a polymer matrix. As discussed in [18–21], LDSLs can be also easily combined with SCs.

The review presented above demonstrates that design and investigation of SCs, which can be mounted together with LSC slabs or coated by LDSL layers, are a real way to achieve the progress in PE production. In this work, Si-based SCs with both horizontal and vertical *p-n* junctions are designed and studied. A module containing a SC with vertically oriented p-n junctions that collects light re-emitted by NCs located in LDSL is proposed. Use of an LDSL is expected to increase the PCE of the SC module up to 10% on large areas. Application of an LDSL as encapsulation material, instead of the commonly used ethylene vinylacetate (EVA), is a key factor to ensure optical coupling between LSC slabs and SCs.

2. Experiment

2.1. Sample design

P-type Si wafers 0.01 m × 0.01 m in size with the resistivity of 0.1 Ohm × m were taken as initial material. All samples were grouped in the series of 10 samples for each of the sizes (for instance Sx.1, Sx.2, Sx.3) to achieve statistical reliability of obtained results. Fabrication of SCs requires wafer cleaning and texturing. In this work, Si wafers were cleaned in a wet chemical bath to remove organic contaminants and microcracks from their surfaces. Surface damage was removed by isotropic etching in a concentrated solution of NaOH and deionized H_2O at 70°C for 600 s. The oxide layer was removed by etching in a solution of HF: H_2O = 1 ml/50 ml for 180 s.

A three-stage plasma treatment was applied to manufacture a single SC. At the first stage, reactive ion etching was carried out using CF_6 and Ar plasma in a PlasmaLab 80 device to decrease the thickness of the *p*-type Si wafer to the thickness corresponding to the light absorption depth in Si (10^{-4} m), as well as remove the surface broken layer, reduce elastic strain in the wafer, and decrease recombination of charge carriers in the wafer bulk [22].

At the second stage, a *p-n* junction was created according to the standard procedure. The sample was etched through the mask to form a 0.3×10^{-6} m deep cuvette. The upper contact n^+-layer was created by thermal diffusion of phosphorus. Next, the *n*-type layer was formed by also using thermal phosphorous diffusion. After the fabrication of the *p-n* junction, ohmic contacts were made by magnetron sputtering of Ti-Mo-Cu-Ni and Al-Ti-Ni stacks on the back and front sides, respectively. A thick Al coating was deposited as a continuous backside electrode. Before measurements, up and down contacts were polished by GaIn paste to ensure the best possible connection with mechanical wires.

Finally, the formed p-n junction was cleaned by directional plasma etching at the third stage of plasma treatment.

Cross-sections of a typical Si-based SC and proposed module are shown in Fig. 1. Fig. 1a presents an SC (S1 series) with an additional jumper serving as a supporting electrode to reduce the SC series resistance. In Fig. 1b, a "cuvette-like concept" (S2 series) is illustrated. An SC with a cuvette can be filled with a luminophore. For this, no jumper is needed. Fig. 1c illustrates the idea of the module, in which several SC elements are connected in a series and attached to the "adaptive window". Moreover, a CdTe/CdS-based polymer film can be used itself as glue to bind all the SCs' elements together.

A planar-type plasma chemical reactor with a magnetic field of cork-like configuration was used for treatment of the surface of the SCs before dip coating CdTe/CdS core shell NCs in the polymer matrix. Plasma etching in a controlled magnetic field enables simultaneous control of the etching rates of the side walls and the surface. The magnetic field was directed parallel to the surface of the electrodes. The process parameters were as follows: $I_d = 2$ A, generator output power W = 150 W, P = 8 Pa, magnetic field strength $H \approx 1.2 \times 10^4$ A/m, and bias voltage $U_{bias} = -60$ V. Hydrogen with purity of 99.9999% was used for the radio frequency treatment at 13.56×10^6 Hz. The reflected power did not exceed 5 W.

2.2. Synthesis method

The synthesis method of CdTe/CdS core/shell NCs with the required sizes was proposed in [19]. This method is based on the reaction of cadmium thioglycolate and hydrogen telluride in an alkaline medium followed by heat treatment of the clusters obtained in this reactionto grow NCs. We synthesized colloidal solutions of CdTe/CdS NCs stabilized by thioglycolic acid. For synthesis of the cadmium precursor solution, 7.95×10^{-4} kg of $3CdSO_4 \times 8H_2O$ was dissolved in 100 ml of distilled water and mixed with 0.87×10^{-4} m^3 of thioglycolic acid (TGA) from Sigma-Aldrich. This mixture was titrated by 1 M sodium hydroxide until a pH value equal to 11 was obtained [20]. Oxygen was removed by bubbling argon through the cadmium precursor solution for 900 s. Hydrogen telluride (H_2Te) produced by electrochemical reduction of tellurium on the tellurium cathode was used as a Te^{2-} source. H_2Te passed through the cadmium precursor solution carried by argon flow. CdTe NCs were formed and then heated to 100°C in order to form the CdS shell, passivate the surface with a stabilizer and enlarge the NCs by thermolysis of cadmium thioglycolate and Ostwald ripening. Three 2×10^{-6} M solutions of CdTe/CdS NCs with different diameters obtained at different heating times (0.5, 6 and 26 hours) were used for investigations. The obtained NCs were negatively charged due to dissociation of TGA molecules.

To measure the optical characteristics of the obtained structures, glass substrates were used as references. The glass substrates were preliminarily treated with a mixture of 96% H_2SO_4 and 30% H_2O_2 at a ratio of 3:1 in order to increase their hydrophilicity by surface hydroxylation. Using the dip coating layer-by-layer deposition process, multilayer polymer films with embedded NCs were deposited on the references and the SCs. This technique is based on electrostatic assembly of oppositely-charged materials, which are polycation poly(dimethyldiallylammonium chloride) (PDDA) and TGA-stabilized CdTe/CdS NCs in our case. The glass substrates and the SCs were immersed vertically in turn according to the following sequence: immersing in 0.2% PDDA solution (300 s), washing off the excess PDDA with distilled water (10 s), immersing in the solution of NCs (300 s), and washing off the excess NCs solution with distilled water (10 s). By repeating this cycle 20 times, a composite sandwich structure consisting of 20 bilayers of PDDA-CdTe/CdS was obtained. The starting 20 wt% aqueous solution of PDDA with an average high molecular weight 400.000–500.000 (409030) was acquired from Sigma-Aldrich. The pH value of the CdTe/CdS solution was in the range of 7.5 to 8.

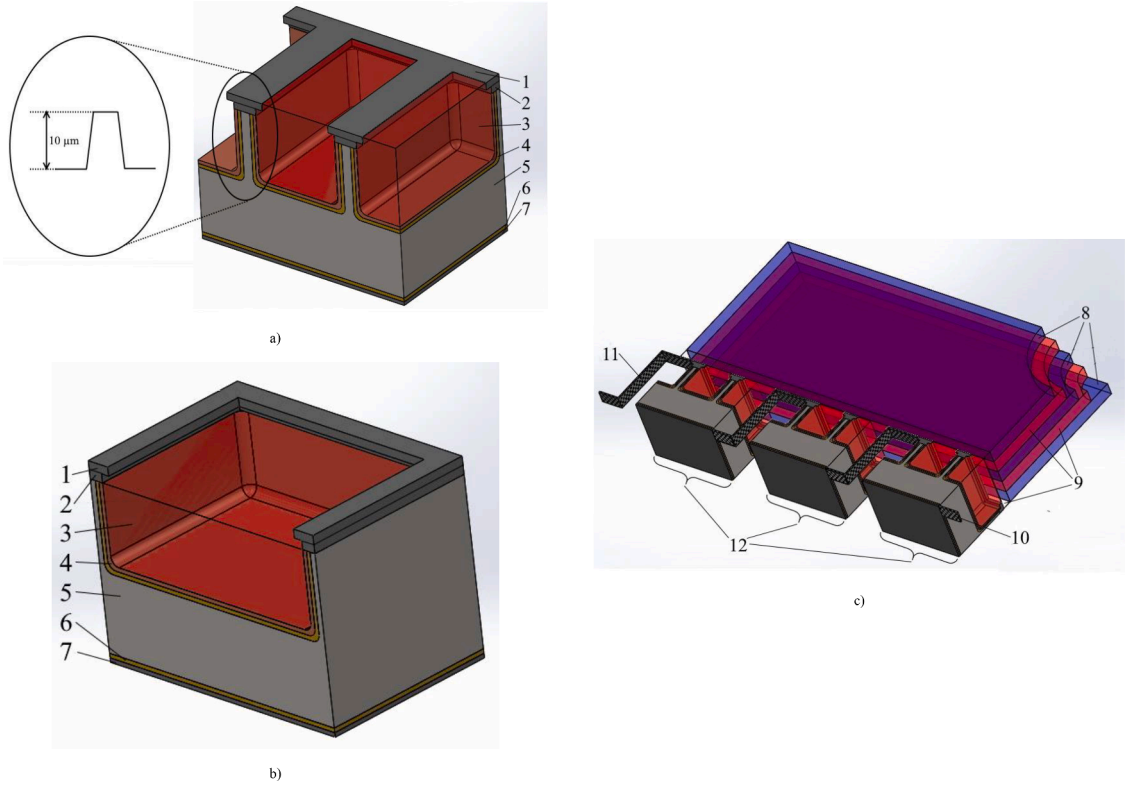

Fig. 1. Si-based solar cells with LDSLs: 1 – Upper metal grid (Ti-Mo-Cu-Ni); 2 – diffusion n^{++}-layer doped with P to 10^{25} m^{-3}; *3* – LDSL coating (less than 3 μm); 4 – diffusion n^{+}-layer doped with P to 3-5 × 10^{24} m^{-3}; 5 – *p*-Si base doped with B to obtain the resistivity of 0.1 Ohm × m. It has the (111) orientation and the thickness of 350 × 10^{-6} m, which is then reduced to 100 × 10^{-6} m; 6 – diffusion p^{+}-layer doped with B to 3-5 × 10^{25} m^{-3}; 7 – bottom metal coating (Al-Ti-Ni), 8 – glass, 9 – LDSL, 10 – anode, 11 – cathode, 12 – prototypes of *p*-Si based SCs with LDSLs: a) S1 series; b) S2 series; c) proposed concept of "adaptive window" with LDSL for SCs.

2.3. Current-voltage characteristics

Current-voltage (*I-U*) characteristics of SCs were measured by four-probe method using a Keithley-2410h. *I-U* characteristics of Si-based SCs under light illumination normalized to the AM1.5 Global spectrum condition with 1000 W/m^2 incident light power were obtained by compensation technique using a 4000 W quartz halogen linear bulb as an external pulsed light source. The intensity of incident light was reduced by normal grey (NG) and metallic grid filters. The transmittance spectra of filters are provided in Fig. 2. The power of photon flux and the temperature of irradiated holder were controlled by a matrix of color sensors (RGBC digital sensor with I2C interface) as well as thermal and UV sensors. A 0.04 m Plexiglas filter was applied to cut off IR radiation. The results we obtained, such as short circuit current, open circuit voltage and maximum power value, were extrapolated using the regression method, the least squares method and the recursive algorithm realized in MathCad. For the two-diode model, the Levenberg-Merquardt curve-fitting technique was applied to simulate *I-U* curves. The simulated curves were fixed when the correlation coefficient R^2 for fitted and measured curves built in logarithmic coordinates did not exceed 10%. The principle of the simulation we used is described in [22]. Based on the simulated results, the values of the shunt and the series resistance of the SCs were calculated. The principle of the calculation of these characteristics is described in the Results and discussion section below.

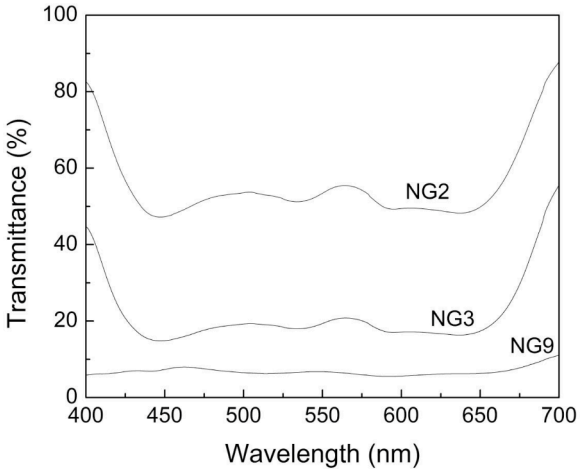

Fig. 2. Transmittance spectra of NGs filters used in this study.

2.4. Photoluminescence measurements

Photoluminescence (PL) measurements were carried out at room temperature in the wavelength range from 450 to 750 nm using a Perkin-Elmer LS55 PL spectrometer. The measurement error was less than 0.5 nm. An excitation light source with $\lambda = 400$ nm and emittance of 0.05 W/m^2 was used. To estimate the size of CdTe/CdS NCs and to obtain the information about their defect structure, optical density (OD) measurements were carried out. The proximity of PL peak position to the fundamental edge of the studied objects points to a small concentration of shallow donors, which are presumably non-radiative recombination centers. OD and PL characteristics were measured synchronously to find the samples with the lowest non-radiative recombination to be used for coating the SCs.

2.5. Optical measurements

A two-beam Specord 210 spectrophotometer was used for

measurements of transmission in the UV and visible spectral ranges. The spectral range from 190 to 1100 nm was probed with a resolution of 0.5/1/2/4 nm. Wavelength calibration with a holmium oxide filter ensured high accuracy and reproducibility of measurement results. WinASPECT software (Win ASPECT® Plus 2.2.1.0, Analytik Jena AG, Germany) with included additional modules significantly enhanced the capabilities of the spectrophotometer.

2.6. Film thickness measurements

Film thicknesses were measured by a microinterferometer MII-4, a Tencor Instruments Alfa Step 1000 profilometer, and an ultra-optimeter technical microscope (contact optical microscope with resolution of 200 nm). Measurements of sample surfaces were done by an Atomic Power Microscope NanoScope IIIaDimension 3000™ from Digital Instruments (supported by Losing Veeco Corp.) in the periodic contact mode using the NSG-11 needle with the radius of 10 nm.

3. Results and discussion

3.1. Photoluminescence

Figs. 3a and 3b shows PL spectra of the structures under investigation. One can see well-resolved luminescence bands peaked at 548, 609 and 642 nm for the S1.1 (2.8 nm), S1.2 (3.6 nm) and S1.3 (4.0 nm) series of samples, respectively. It can be seen that the PL peaks are red-shifted in the case of longer heating. This can be attributed to the decrease of band gap energy due to the increase of NC diameters. Besides, non-

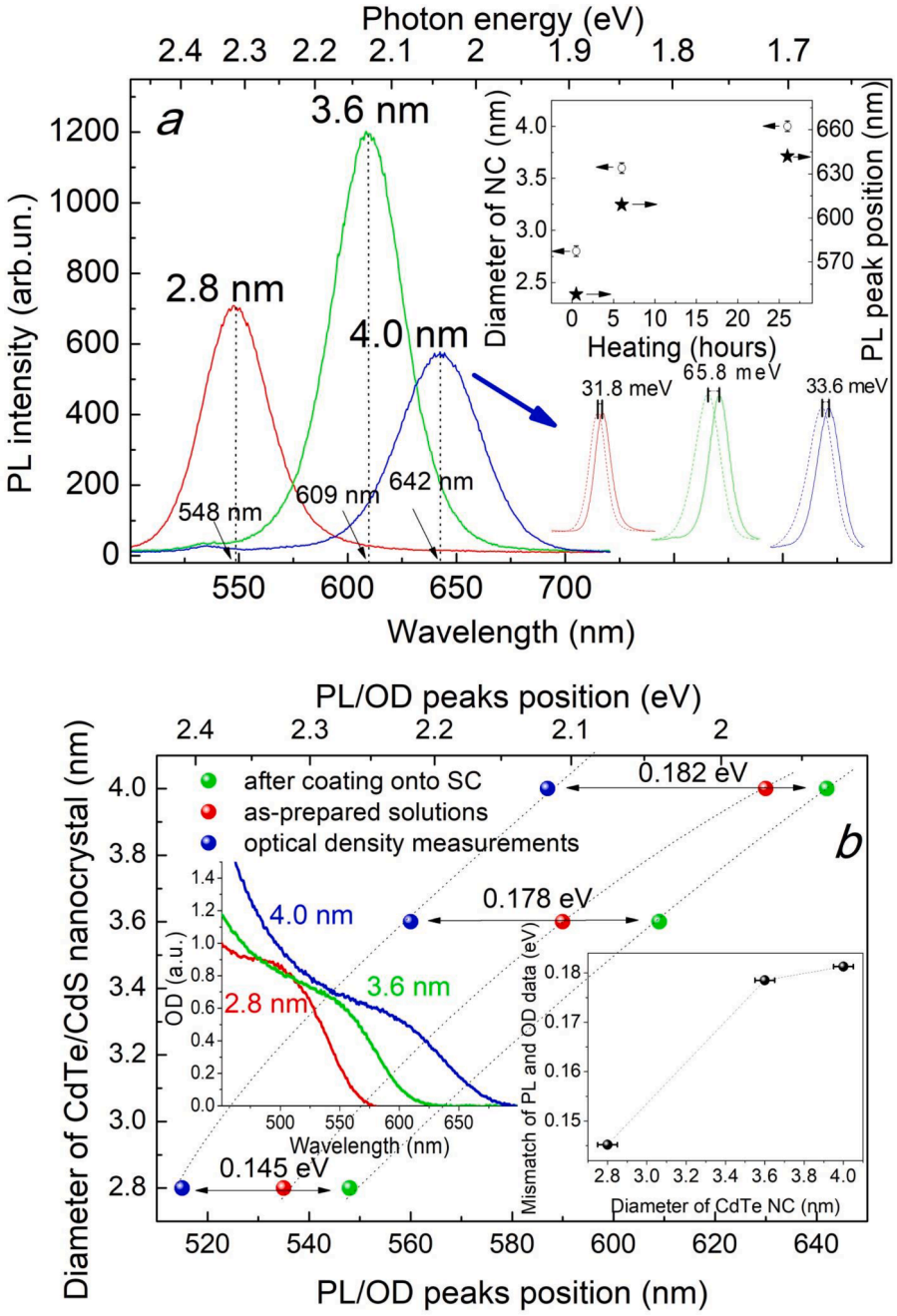

Fig. 3. PL spectra of colloidal solutions with CdTe/CdS NCs. a) PL spectra and shift of peak position of LDSL with various NC sizes. In the inset: dependence of NC size (empty circles) and PL peak position (stars) on the time of heating, b) Dependence of PL/OD on NC size. In the insets: OD spectra of NCs (left) and mismatch of PL and OD peak positions vs. NC size (right).

monotonous changes of band intensities can be seen, which correlate with the observations reported in [21,23]. The shift of peak position as a result of the increase of heating time is not linear (see inset in Fig. 3a), while the dependence of NC diameter on the PL peak position appears linear with a small curvature (Fig. 3b). One can see that for CdTe/CdS NCs, PL is peaked at much smaller energies as compared to the absorption peak position (left inset in Fig. 3b). This indicates the presence of defects in such NCs. These defects are usually related to surface non-radiative recombination centers and can be passivated to yield relatively efficient PL [24]. Moreover, some deep trap states related to internal crystal defects can play a significant role as non-radiative recombination centers [21]. The same energy of the absorption edge and PL peak verifies band edge emission and signifies absence of deep states and/or shallow levels within the band gap of semiconductor.

The samples under investigation are characterized by different positions of OD and PL peaks in as-prepared solutions as well as by a red-shift of PL spectra after coating onto the SCs. This implies that non-radiative recombination defects are present in these samples. Except for already noticed surface and deep-center non-radiative recombination, Auger recombination is another channel of the non-radiative transitions of free carriers. To ensure high emission quality of the coating layer, non-radiative recombination should be suppressed to the highest possible extent.

It should be noticed that different research groups observed the same OD peaks at different NC sizes. Apparently, this is caused by the measurement errors mainly related to the determination of NC sizes and distribution (transmission electron microscopy and/or X-ray diffraction measurements followed by size calculation by Debye-Scherrer formula [21,25,26]). In [27], an empirical fitting function for CdTe/CdS NCs was obtained based on the analysis of a number of works:

$$D = \left(9.8127\cdot10^{-7}\right)\lambda^3 - \left(1.7147\cdot10^{-3}\right)\lambda^2 + (1.0064)\lambda - (194.84), \quad (1)$$

where D (nm) is the NC diameter and λ (nm) is the wavelength of the first excitonic absorption peak, respectively. We used this expression for estimation of the diameters of the NCs in our cases. At the same time, the authors of [27] argue that their relation may become invalid in the size ranges not covered by the collected data. The general approach to estimate the sizes of the NCs is based on the effective mass approximation [28–30]. According to [31]:

$$E(d) = \frac{2\hbar^2\pi^2}{d^2}\left(\frac{1}{m_e^*} - \frac{1}{m_h^*}\right) - \frac{3.572e^2}{\varepsilon d} - \frac{0.124e^4}{\hbar^2\varepsilon^2}\left(\frac{1}{m_e^*} + \frac{1}{m_h^*}\right)^{-1}, \quad (2)$$

where m_e^* and m_h^* are the electron and hole effective masses, respectively, and d and ε are the diameter and the dielectric constant of the semiconductor, respectively. The first term in expression (2) is the kinetic energy of an electron and a hole. The second term describes their Coulomb attraction. The last term corresponds to the correlation between the two particles. It was noticed in [30] that this expression is appropriate when electrons and holes are practically uncorrelated ($d \sim 4$ nm) and can be considered as individual particles. However, for the smallest NC sizes, use of expression (2) fails due to the over-simplification of the description of crystal potential. The authors of [30] proposed a tight-binding model for this case but no explicit formula was provided. One may use the Brus equation, which is also based on the effective mass approximation and looks as follows [28,29,32]:

$$E = E_g^{bulk} + \frac{\hbar^2\pi^2}{2er^2}\left(\frac{1}{m_e^* m_0} + \frac{1}{m_h^* m_0}\right) - \frac{1.8e}{4\pi\varepsilon\varepsilon_0 r} - \frac{0.124e^3}{\hbar^2(4\pi\varepsilon\varepsilon_0)^2}\left(\frac{1}{m_e^* m_0} + \frac{1}{m_h^* m_0}\right)^{-1}, \quad (3)$$

where E_g^{bulk} is the band gap of bulk material and $2r$ is the diameter of nanoparticle. The key prediction of all presented expressions is the red-shift of absorbance peak position with the increase of NC diameter. Therefore, the observed red-shifts of OD and PL peak positions are apparently related to the increase of the diameters of the NCs. No OD signal from NCs was detected after coating NCs onto an SC, but the PL peak position red-shifted (~ 30 – 60 meV for different peaks, see Fig. 3a). Furthermore, the mismatch between the OD and the shifted PL peaks became more significant (see inset in Fig. 3b). Moreover, this mismatch looks like saturation at increased NC diameters. This feature points to the increase of the number of defect states with the increase of NC diameter.

The effective LDSL coating for SCs should have a high PL quantum yield. However, presence of shallow energy levels in the band gap of semiconductor results in the absorption of high-energy and emission of low-energy photons. This emission results in the necessity to increase the light intensity for SC operation. To increase the efficiency of SCs, the energy of emitted photons should be close to the energy of the band gap of semiconductor material that makes up the base of an SC. Unfortunately, after the coating of an SC, apparent modification of NCs is observed. This fact is evidenced by the shift of observed PL peaks (Fig. 3b). A small red-shift can be explained by the increase of shell thickness (CdS) due to possible photo-chemical reactions and impurity accumulation. To reach the best results (unchanged spectral characteristics after coating onto an SC), a better-quality polymer matrix, which would preserve NCs for a long time without transformation, is required.

3.2. Current-voltage characteristics of SCs

Analysis of *I-U* characteristics under illumination allows us to determine the series and the shunt resistance. The calculation method of the series resistance is presented by the following expressions:

$$R_s = \frac{R_1 + R_2 + R_3}{3},$$
$$R_1 = \frac{U_2 - U_1}{Isc_1(U_1) - Isc_2(U_2)}; R_2 = \frac{U_3 - U_2}{Isc_2(U_2) - Isc_3(U_3)}; R_3 = \frac{U_3 - U_1}{Isc_1(U_1) - Isc_3(U_3)}, \quad (4)$$

where U_1, U_2, U_3 are the values of voltage at maximum power values (P_{max}) and Isc_1, Isc_2, Isc_3 are the interpolated values of the short circuit current at different values of P_{max}. Various NG filters as well as metallic grids were applied to decrease the incident light flux to order different points of P_{max}. For the calculation method, the values of P_{max} should be as far apart as possible, therefore the name of the NG is not critical. NG glass filters are generally used in optical experiments; unlike NG filters, metallic grids have linear optical transmittance. In our case, grids were applied to choose NG filters with the best linearity of spectral transmittance in visible optical range, see Fig. 2.

The series resistance was calculated by expression (4) using the values of voltage and short circuit current that corresponded to the points of P_{max} for each sample. The value of shunt resistance was determined by calculation of the slope of the linear segment of the *I-U* curve close to I_{SC}. The minimum value of applied voltage on the *I-U* characteristics under illumination (see (5)) is expressed as follows:

$$R_{sh} = -\frac{1}{dI_{SC}/dU}. \quad (5)$$

The results of the calculations of series and shunt resistances are presented in Table 1. Fig. 4 shows *I-U* characteristics of S1-concept SCs with LDSL composed by CdTe/CdS NCs measured under light conditions. SCs according to the S2 concept are better compatible with LDSLs. However, such SCs did not show effective PE because of the absence of a jumper, the role of which is to reduce the series resistance and increase the current flow during PE generation. The curve 1 in Fig. 4 corresponds to the *I-U* characteristic of the initial SC. As can be further seen from this figure, the curve 2 for the sample S1.1 (NC diameter of 2.8 nm) is not a typical *I-U* characteristic of an SC. Therefore, PCE and other parameters cannot be calculated for it because the correlation coefficient between

Table 1
Measured parameters of solar cells with CdTe/CdS NCs based LDSLs on an area of $1 \times 1 \times 10^{-4}$ m^2.

	N	*S*, nm	U_{oc}, mV	I_{sc}, mA	P_{max}, *W*	U_{max}, mV	I_{max}, *mA*	*FF*	*Ef.* %	R_s, Ohm	R_{sh}, Ohm
1	Int		461	22	6.15×10^{-3}	345	18	0.615	6.12	1.5	476
2	S1.1	2.8	Determination is impossible (correlation coeff. > 10%)								
3	S1.2	3.6	483	33	8.58×10^{-3}	323	27	0.562	8.85	2.9	420
4	S1.3	4.0	484	35	8.95×10^{-3}	316	28	0.521	8.92	3	367.6

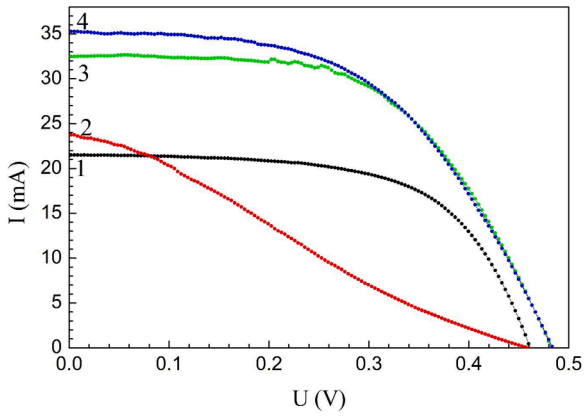

Fig. 4. *I-U* characteristics under light illumination of p-Si based SCs with LDSLs measured under AM1.5 condition: 1 – Initial (concept S1), 2 - S1.1 (2.8 nm), 3 - S1.2 (3.6 nm), 4 - S1.3 (4 nm).

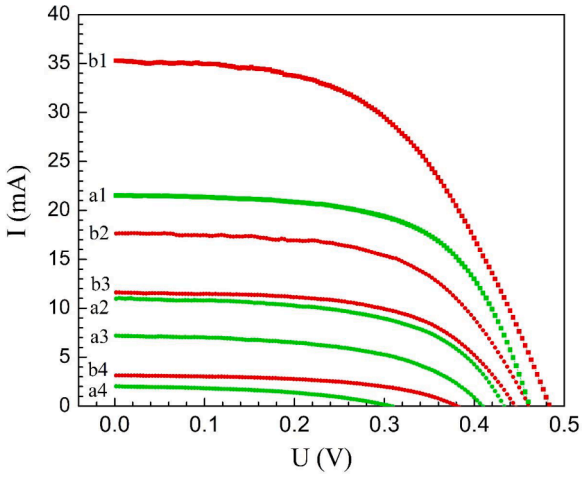

Fig. 5. *I-U* characteristics under light illumination of p-Si based S1.3 (4 nm) SCs measured under AM1.5 condition and with normal gray filters (NG): a1) - AM1.5, a2) - NG2, a3) - NG3, a4) - NG9. The same characteristics of SCs with LDSLs: b1) - AM1.5, b2) - NG2, b3) - NG3, b4) - NG9.

the simulated and measured curves is more than 50%. In accordance with this, an empty line is left in Table 1. Such a behavior of an *I-U* curve can be due to the following reasons. The light re-emitted by 2.8 nm NCs has the close to the low photon energy (red light). As the photon energy increases, absorption in the SC base material (Si in our case) begins to play a more significant role. That is, a substantial portion of photons recombines even before reaching the p-n junction. Moreover, the NCs themselves partially shield the SC from photons that can be absorbed, while re-emission does not compensate for this effect. The curves 3 and 4 for S1-concept SCs measured for the structures with NC sizes of 3.6 and 4.0 nm almost coincide over the entire voltage range. As a result, the short-circuit current value corresponding to the curve 4 is higher. This may be caused by the fact that the maximum voltage of the SC under no-load condition was reached in our configuration, e.g. due to better connection of bigger NCs inside the LDSL with the surface of p-n junction.

Fig. 5 presents *I-U* characteristics of the S1-concept SC with LDSL containing 4.0 nm CdTe/CdS NCs measured under light conditions using various NG filters. Series resistance is known to limit the short circuit current value. In our case, the short circuit current of the SC increased due to light re-emission by NCs located in the luminophore. Unavoidable leakage of current on SC surfaces is taken into account by shunt resistance. The influence of the latter on the behavior of current flow results in a slight decrease of the open circuit voltage (U_{oc}) and an increase of the slope of the *I-U* curve. This effect is caused by the increase of the effective area of the SC, which leads to the increase of parasitic leakages. Analysis of the *I-U* characteristics under illumination (Figs. 4 and 5) and the results summarized in Table 1 enables us to conclude that U_{oc} and PCE of the SCs improved with the increase of the diameter of the CdTe/CdS NCs. The SC demonstrating the best results contained CdTe/CdS NCs 4.0 nm in diameter.

As can be seen from Table 1, SCs with CdTe/CdS NC-based films as "adaptive window" layers have a short circuit current density (J_{sc}) of 35 mA/cm^2, $U_{oc} = 0.48$ V, a fill factor (FF) equal to 52.1%, and the highest PCE of 8.98%. In contrast to that, the initial SCs without such films demonstrate PCE of 6.1% and FF = 61.5%. Low values of the FF of coated SCs were mainly due to the intense carrier recombination at the p-n junction interface [34,35]. Our PCE values are superior to those of the best SC devices with CdTe/CdS reported in [33] (5.14%) and [34] (5.6 – 5.9%).

4. Conclusion

Solar cells with luminescent solar concentrating layers (LDSL type) containing CdTe/CdS nanocrystals were fabricated. Double aligned (both horizontally and vertically oriented) p-n junction solar cells with the architecture of (Ti-Mo-Cu-Ni)/(CdS-CdTe)/(P-doped n^{++}-layer)/(P-doped n^{+}-layer)/(B-doped p-Si)/(B-doped p^{+}-layer)/(Al-Ti-Ni) were designed. Luminescent solar concentrating LDSLs were constructed according to the design of luminescent down shifting layers with the average diameters of the CdTe/CdS nanocrystals of 2.8, 3.6 and 4.0 nm. The CdTe/CdS nanocrystals were stabilized by thioglycolic acid. They were synthesized in aqueous solution and dip coated onto the surface of solar cells using the layer-by-layer deposition technique. The influence of photoluminescence on the efficiency of solar cells was studied and discussed in detail. The photoluminescence bands peaked at 548, 609 and 642 nm for samples of the series S1.1 (2.8 nm), S1.2 (3.6 nm) and S1.3 (4 nm), respectively. We revealed mismatches in the positions of the optical densities and photoluminescence peaks of CdTe/CdS nanocrystals in as-prepared solutions and after coating onto the solar cell surfaces. These mismatches became more pronounced with the increase of nanocrystal diameter, which might signify the increase of the number of defect states. Photoluminescence peaks were more red-shifted for longer heating times during the nanocrystal preparation. Furthermore, these peaks further red-shifted after coating onto the solar cells. This effect could be attributed to the increase of CdS-shell thickness due to possible photo-chemical reactions. Analysis of the current-voltage characteristics enabled us to conclude that open circuit voltage and power conversion efficiency of solar cells were improved upon increasing the diameter of CdTe/CdS nanocrystals. Solar cells with the S1.3 coating layer (nanocrystal size of 4.0 nm) demonstrated short

circuit current density of 35 mA/cm^2, open circuit voltage of 0.48 V, a fill factor of 52.1%, and the highest observed power conversion efficiency of 9% on an area of 1 cm^2.

CRediT authorship contribution statement

M. Semenenko Conceptualization, Investigation, Validation, Writing – original draft, Writing – review & editing Methodology. **R. Redko** Investigation of Photoluminescence, Validation, Writing – original draft Writing – review & editing. **A. Sarikov** Validation, Writing – review & editing. **G. Okrepka** Resources, Investigation, Dip-Coating Deposition, Thin Films Creation, Writing – original draft. **V. Shvalagin** Investigation, Chemistry Analyses. **M. Dusheiko** Resources, Solar Cell Module Technology Production. **V. Hladkovskyi** Investigation, Plasma Treatment. **S. Antonin** Investigation, Current-Voltage Characterization, Designing. **F. Gao** Resources. **S. Shahan** Resources, Optical Characterization.

Declaration of Competing Interest

The authors declare that they have no known competing financial interests or personal relationships that could have appeared to influence the work reported in this paper.

Data availability

Data will be made available on request.

References

[1] P. Moraitis, R.E.I. Schropp, W.G.J.H.M. van Sark, Nanoparticles for luminescent solar concentrators - a review, Opt. Mater. 84 (2018) 636–645, https://doi.org/10.1016/j.optmat.2018.07.034.

[2] A. Reinders, R. Kishore, L. Slooff, W. Eggink, Luminescent solar concentrator photovoltaic designs, Jpn. J. Appl. Phys. 57 (2018) 08RD10, https://doi.org/10.7567/JJAP.57.08RD10.

[3] H. Zhao, D. Benetti, X. Tong, H. Zhang, Y. Zhou, G. Liu, D. Ma, S. Sun, Z.M. Wang, Y. Wang, F. Rosei, Efficient and stable tandem luminescent solar concentrators based on carbon dots and perovskite quantum dots, Nano Energy 50 (2018) 756–765, https://doi.org/10.1016/j.nanoen.2018.06.025.

[4] Z. Krumer, W.G.J.H.M. van Sark, R.E.I. Schropp, C. de Mello Donegá, Compensation of self-absorption losses in luminescent solar concentrators by increasing luminophore concentration, Sol. Energy Mater. Sol. Cells 167 (2017) 133–139, https://doi.org/10.1016/j.solmat.2017.04.010.

[5] E.P.J. Merkx, O.M. Ten Kate, E. van der Kolk, Rapid optimization of large-scale luminescent solar concentrators: evaluation for adoption in the built environment, Opt. Express 25 (2017) A547–A563, https://doi.org/10.1364/OE.25.00A547.

[6] E.P.J. Merkx, M.P. Plokker, E. van der Kolk, The potential of transparent sputtered NaI:Tm^{2+}, $CaBr_2$:Tm^{2+}, and CaI_2:Tm^{2+} thin films as luminescent solar concentrators, Sol. Energy Mater. and Sol. Cells 223 (2021), 110944, https://doi.org/10.1016/j.solmat.2020.110944.

[7] W.H. Weber, J. Lambe, Luminescent greenhouse collector for solar radiation, Appl. Opt. 15 (1976) 2299, https://doi.org/10.1364/AO.15.002299.

[8] G. Iasilli, R. Francischello, P. Lova, S. Silvano, A. Surace, G. Pesce, M. Alloisio, M. Patrini, M. Shimizu, D. Comoretto, A. Pucci, Luminescent solar concentrators: boosted optical efficiency by polymer dielectric mirrors, Mater. Chem. Front. 3 (2019) 429–436, https://doi.org/10.1039/C8QM00595H.

[9] R. Reisfeld, New developments in luminescence for solar energy utilization, Opt. Mater. 32 (2010) 850–856, https://doi.org/10.1016/j.optmat.2010.04.034.

[10] C. Yang, D. Liu, A. Renny, P.S. Kuttipillai, R.R. Lunt, Integration of near-infrared harvesting transparent luminescent solar concentrators onto arbitrary surfaces, J. Lumin. 210 (2019) 239–246, https://doi.org/10.1016/j.jlumin.2019.02.042.

[11] L.H. Slooff, E.E. Bende, A.R. Burgers, T. Budel, M. Pravettoni, R.P. Kenny, E. D. Dunlop, A. Büchtemann, A luminescent solar concentrator with 7.1% power conversion efficiency: carbon nanotube/epoxy resin composites using a block copolymer as a dispersing agent, Phys. Stat. Sol. (RRL). 2 (2008) 257–259, https://doi.org/10.1002/pssr.200802186.

[12] X. Gong, W. Ma, Y. Li, L. Zhong, W. Li, X. Zhao, Fabrication of high-performance luminescent solar concentrators using N-doped carbon dots/PMMA mixed matrix slab, Org. Electron. 63 (2018) 237–243, https://doi.org/10.1016/j.orgel.2018.09.028.

[13] B.R. Sutherland, Cost competitive luminescent solar concentrators, Joule 2 (2018) 203–204, https://doi.org/10.1016/j.joule.2018.02.004.

[14] H. Yang, C. Huang, X. Li, R. Shi, K. Zhang, Luminescent and photocatalytic properties of cadmium sulfide nanoparticles synthesized via microwave irradiation, Mater. Chem. Phys. 90 (2005) 155–158, https://doi.org/10.1016/j.matchemphys.2004.10.028.

[15] C. Strümpel, M. McCann, G. Beaucarne, V. Arkhipov, A. Slaoui, V. Švrček, C. del Cañizo, I. Tobias, Modifying the solar spectrum to enhance silicon solar cell efficiency—an overview of available materials, Sol. Energy Mater. Sol. Cells 91 (2007) 238–249, https://doi.org/10.1016/j.solmat.2006.09.003.

[16] N.I. Klyui, M.A. Semenenko, I.M. Khatsevich, A.V. Makarov, A.N. Kabaldin, F. V. Fomovskii, W. Han, Improvement in the degradation resistance of silicon nanostructures by the deposition of diamond-like carbon films, Semiconductor 49 (2015) 1030–1034, https://doi.org/10.1134/S1063782615080126.

[17] M.B. de la Mora, O. Amelines-Sarria, B.M. Monroy, C.D. Hernández-Pérez, J. E. Lugo, Materials for downconversion in solar cells: perspectives and challenges, Sol. Energy Mater. Sol. Cells 165 (2017) 59–71, https://doi.org/10.1016/j.solmat.2017.02.016.

[18] S. Kalytchuk, S. Gupta, O. Zhovtiuk, A. Vaneski, S.V. Kershaw, H. Fu, Z. Fan, E.C. H. Kwok, C.-F. Wang, W.Y. Teoh, A.L. Rogach, Semiconductor nanocrystals as luminescent down-shifting layers to enhance the efficiency of thin-film CdTe/CdS and crystalline Si solar cells, J. Phys. Chem. C 118 (2014) 16393–16400, https://doi.org/10.1021/jp410279z.

[19] A.L. Rogach, D. Nagesha, J.W. Ostrander, M. Giersig, N.A. Kotov, Raisin bun"-type composite spheres of silica and semiconductor nanocrystals, Chem. Mater. 12 (2000) 2676–2685, https://doi.org/10.1021/cm000244i.

[20] N. Doskaliuk, Y. Khalavka, P. Fochuk, Influence of the shell thickness and ratio between core elements on photostability of the CdTe/CdS core/shell quantum dots embedded in a polymer matrix, Nanoscale Res. Lett. 11 (2016) 216, https://doi.org/10.1186/s11671-016-1428-3.

[21] M. Marandi, B. Emrani, H. Zare, Synthesis of highly luminescent CdTe/CdS core-shell nanocrystals by optimization of the core and shell growth parameters, Opt. Mater. 69 (2017) 358–366, https://doi.org/10.1016/j.optmat.2017.04.058.

[22] M.O. Semenenko, M.G. Dusheiko, S.V. Mamykin, V.O. Ganus, M.V. Kirichenko, R. V. Zaitsev, M.M. Kharchenko, N.I. Klyui, Effect of plasma, RF, and RIE treatments on properties of double-sided high voltage solar cells with vertically aligned p-n Junctions, Int. J. Photoenergy 2016 (2016), 1815205, https://doi.org/10.1155/2016/1815205.

[23] L. Jing, S.V. Kershaw, T. Kipp, S. Kalytchuk, K. Ding, J. Zeng, M. Jiao, X. Sun, A. Mews, A.L. Rogach, M. Gao, Insight into strain effects on band alignment shifts, carrier localization and recombination inetics in CdTe/CdS core/shell quantum dots, J. Am. Chem. Soc. 137 (2015) 2073–2084, https://doi.org/10.1021/ja5127352.

[24] T. Rajh, O.I. Micic, A.J. Nozik, Synthesis and characterization of surface-modified colloidal cadmium telluride quantum dots, J. Phys. Chem. 97 (1993) 11999–12003, https://doi.org/10.1021/j100148a026.

[25] F.T.L. Muniz, M.A.R. Miranda, C. Morilla dos Santos, J.M. Sasaki, The Scherrer equation and the dynamical theory of X-ray diffraction, Acta Crystallogr. A Found Adv.. 72 (2016) 385–390, https://doi.org/10.1107/S205327331600365X.

[26] K. He, N. Chen, C. Wang, L. Wei, J. Chen, Method for determining crystal grain size by X-ray diffraction, Cryst. Res. Technol. 53 (2018), 1700157, https://doi.org/10.1002/crat.201700157.

[27] W.W. Yu, L. Qu, W. Guo, X. Peng, Experimental determination of the extinction coefficient of CdTe, CdSe, and CdS nanocrystals, Chem. Mater. 15 (2003) 2854–2860, https://doi.org/10.1021/cm034081k.

[28] L.E. Brus, A simple model for the ionization potential, electron affinity, and aqueous redox potentials of small semiconductor crystallites, J. Chem. Phys. 79 (1983) 5566–5571, https://doi.org/10.1063/1.445676.

[29] L.E. Brus, Electron–electron and electron-hole interactions in small semiconductor crystallites: the size dependence of the lowest excited electronic state, J. Chem. Phys. 80 (1984) 4403–4409, https://doi.org/10.1063/1.447218.

[30] P.E. Lippens, M. Lannoo, Calculation of the band gap for small CdS and ZnS crystallites, Phys. Rev. B 39 (1989) 10935–10942, https://doi.org/10.1103/PhysRevB.39.10935.

[31] Y. Kayanuma, Wannier exciton in microcrystals, Solid State Commun. 59 (1986) 405–408, https://doi.org/10.1016/0038-1098(86)90573-9.

[32] R.K. Katiyar, S. Sahoo, A.P.S. Gaur, A. Singh, G. Morell, R.S. Katiyar, Studies of photovoltaic properties of nanocrystalline thin films of CdS–CdTe, J. Alloy. Compd. 509 (2011) 10003–10006, https://doi.org/10.1016/j.jallcom.2011.08.011.

[33] S. Liu, W. Liu, J. Heng, W. Zhou, Y. Chen, S. Wen, D. Qin, L. Hou, D. Wang, H. Xu, Solution-processed efficient nanocrystal solar cells based on CdTe and CdS nanocrystals, Coatings 8 (2018) 26, https://doi.org/10.3390/coatings8010026.

[34] Zhitao Rong, Xiuzhen Guo, Shaoshan Lian, Songwei Liu, Donghuan Qin, Yueqi Mo, Wei Xu, Hongbin Wu, Hong Zhao, Lintao Hou, Interface engineering for both cathode and anode enables low-cost highly efficient solution-processed CdTe nanocrystal solar cells, Adv. Funct. Mater. 29 (2019), 1904018, https://doi.org/10.1002/adfm.201904018.

[35] Qingsen Zeng, Lu Hu, Jian Cui, Tanglue Feng, Xiaohang Du, Gan Jin, Fangyuan Liu, Tianjiao Ji, Fenghong Li, Hao Zhang, Bai Yang, High-efficiency aqueous-processed polymer/CdTe nanocrystals planar heterojunction solar cells with optimized band alignment and reduced Interfacial charge recombination, ACS Appl. Mater. Interfaces 9 (2017) 31345–31351, https://doi.org/10.1021/acsami.7b09901.